ISSN 2070-0504, Catalysis in Industry, 2017, Vol. 9, No. 1, pp. 23–30. © Pleiades Publishing, Ltd., 2017.
Original Russian Text © O.A. Kungurova, N.V. Shtertser, G.K. Chermashentseva, I.I. Simentsova, A.A. Khassin, 2016, published in Kataliz v Promyshlennosti.

DOMESTIC CATALYSTS

Ruthenium Promoted Cobalt–Alumina Catalysts for the Synthesis of High-Molecular-Weight Solid Hydrocarbons from CO and Hydrogen

O. A. Kungurova[a, b, c, *], N. V. Shtertser[b, **], G. K. Chermashentseva[b, *], I. I. Simentsova[b, ****], and A. A. Khassin[a, b, *****]**

[a] *Research and Education Center of Energy-Efficient Catalysis, Novosibirsk National Research University, Novosibirsk, 630090 Russia*

[b] *Boreskov Institute of Catalysis, Siberian Branch, Russian Academy of Sciences, Novosibirsk, 630090 Russia*

[c] *National Research Tomsk State University, Tomsk, 634050 Russia*

**e-mail: olya-sky@inbox.ru*

***e-mail: nat@catalysis.ru*

****e-mail: chgk@catalysis.ru*

*****e-mail: sii@catalysis.ru*

******e-mail: khassinaa@mail.ru*

Received April 25, 2016

Abstract—The effect of the ruthenium promotion of Fischer–Tropsch (FT) cobalt–alumina catalysts on the temperature of catalyst activation reduction and catalytic properties in the FT process is studied. The addition of 0.2–1 wt % of ruthenium reduces the temperature of reduction activation from 500 to 330–350°C while preserving the catalytic activity and selectivity toward C_{5+} products in FT synthesis. FT ruthenium-promoted Co–Al catalysts are more selective toward higher hydrocarbons; the experimental value of parameter α_{ASF} of the distribution of paraffinic products for ruthenium-promoted catalysts is 0.93–0.94, allowing us to estimate the selectivity toward C_{20+} synthetic waxes to be 48 wt %, and the selectivity toward C_{35+} waxes to be 23 wt %. Ruthenium-promoted catalysts also exhibit high selectivity toward olefins.

Keywords: cobalt catalysts, promotion, ruthenium, reductive activation, Fischer–Tropsch synthesis

DOI: 10.1134/S2070050417010081

INTRODUCTION

The synthesis of hydrocarbons from CO and hydrogen, known as Fischer–Tropsch synthesis (FTS), using cobalt catalysts is a promising process in the technological processing of natural gas, the industrial use of which will be expanded in the coming decades. The present composition of the reaction products includes saturated and unsaturated hydrocarbons that range from methane to very long hydrocarbon chains up to C_{60+} and alcohols. The composition of the products conforms very closely to the Anderson–Schulz–Flory molecular weight distribution:

$$M_n = (1-\alpha)\alpha^{(n-1)}, \quad (1)$$

$$W_n \approx \frac{nM_n}{\sum nM_n} = (1-\alpha)^2 n\alpha^{(n-1)}, \quad (2)$$

where M_n is the mole fraction and W_n is the mass fraction of a hydrocarbon with n carbon atoms in the hydrocarbon chain. Parameter α_{ASF} in these expressions (and thus the fractional composition of the products) depend strongly on the catalyst (including the dispersion of the active ingredient [1, 2]) and the process conditions, especially temperature [2–4]. The higher the α_{ASF} value, the greater the mass fraction (or the proportion, expressed on the basis of carbon) of high molecular hydrocarbons that are solid under normal conditions. These are normally referred to as synthetic wax or ceresins (C_{35+}). High yields of ceresins are achieved in processes with high pressures (20 atm or higher), low flow rates of the synthesis gas, and low temperatures (190°C and below) [5]. The processing of heavy hydrocarbons into liquid fractions of distillate diesel, kerosene, and naphtha at refineries requires an additional hydrocracking stage that raises capital costs by about 10%. Some studies [6, 7] suggest avoiding this stage by limiting the α_{ASF} parameter to a range that excludes the formation of the solid hydrocarbon phase. This leads inevitably to an up to 20% increase in the yield of undesirable methane, an up to 55% reduction in selectivity toward the target C_{5+} fraction, and to a substantial increase in unit capital costs each time

the process is performed. In addition, the properties of the resulting liquid product exclude its direct use as motor fuel: low density, poor lubricity, and high cloud points are characteristic of the linear or slightly branched paraffins that constitute more than 90% of the final product [8]. It is therefore advisable to optimize the process to obtain the maximum yield of high-molecular solid hydrocarbons (which can be converted into liquids at the subsequent hydrocracking/hydroisomerization stage, if required).

It is worth noting that synthetic waxes (ceresins) have their own commercial value, and their market value is much higher than that of liquid products. These products can be divided into paraffin fractions with different melting ranges (drop points) through the additional fractionating of waxes. These fractions are similar to oil paraffins: petrolatum (vaseline) with a melting point of 60 °C, along with paraffin and microcrystalline waxes with melting points of 80°C and higher. The predominantly linear molecular geometry of synthetic wax gives it such unusual properties as low viscosity in the liquid state and great hardness in the solid state. We can therefore obtain wax fractions with melting temperatures (dropping points) higher than 100°C, which is very difficult to achieve when petroleum waxes are used. The synthetic waxes obtained via the FT process are currently used to produce hot melt adhesives, inks, paints, coatings, cosmetics (lipstick, creams, and lotions), retarders, and fillers for solid fuels and explosives. In addition, synthetic waxes can be also used instead of traditional (oil) waxes to produce waterproof packaging, paper, cardboard, disposable tableware, water repellent fabrics, suppositories, food packaging, and so on. Their advantage in this case is that there are no aromatic hydrocarbons and naphthenes and, as a result, no color or odor.

Some works [9–12] performed at the Boreskov Institute of Catalysis in Novosibirsk suggest using a cobalt catalyst with high dispersion of the active component (cobalt) and optimum interaction with the carrier (δ-Al_2O_3), ensuring both the high selectivity and high activity of the catalyst. A disadvantage of Co/δ-Al_2O_3 catalysts is the high reduction temperature of cobalt cations from Co-Al oxide to form metal particles above 500°C. If the reductive activation of catalysts composed of Co-Al oxides derived from Co-Al oxyhydroxides is performed at lower temperatures, only a small part of the cobalt is reduced to the metallic state, and the catalysts become inactive [13]. The high temperature of the reduction of the active component (cobalt), which may be considered the last step of catalyst preparation or as a separate process of the reductive activation of the catalyst, leads to considerable difficulties in the industrial use of this catalyst. If activation is performed in a synthesis reactor immediately after it is loaded, the design and materials of the reactor and heat exchange equipment must be stable at temperatures of up to 600°C and more, which is much higher than the synthesis temperature (190–230°C). This greatly increases the cost of a reactor. If activation is performed in a separate apparatus, additional stages of its passivation and conservation are required after activation of the catalyst; loading the catalyst into the reactor becomes complicated (a protective atmosphere is required) and the catalyst is subjected to additional mechanical stress when loaded and unloaded from the activator.

One way of reducing the activation temperature of cobalt catalysts is to introduce noble metals (Pt, Pd, Ru, and Re) into their structure. These promote cobalt reduction up to the metallic state, but platinum and palladium negatively affect its selectivity, revealing intrinsic activity in hydrogenation of CO to form methane and light hydrocarbons [14, 15]. On the other hand, introducing up to 5 wt % of ruthenium only slightly reduces and even improves the selectivity of cobalt catalysts toward high molecular weight hydrocarbons. Several authors have shown that promoting Co-Al_2O_3 catalysts with small amounts of ruthenium lowers cobalt's characteristic reduction temperature by 100–150°C (according to TPR) and improves the initial catalyst's activity to retain selectivity toward C_{5+} products [14–20]. Ruthenium affects the dispersion of the active component's particles: introducing a promoter increases dispersion by two or more times, according to data on hydrogen chemisorption with the subsequent titration of oxygen. The hydrogen chemisorption data indicate [21] that promoting cobalt catalyst does not increase its dispersion; however, transmission electron microscopy data show that the proportion of ultrafine particles (smaller than 6 nm) falls from 83 to 49%, while that of particles in the range of 6–12 nm (the optimum size for FTS) rises from 17 to 51%.

The problem of finding the optimum promoter of Co-Al catalyst to reduce its activation temperature thus remains relevant. In this work, we study the possibility of promoting Co/δ-Al_2O_3 catalyst prepared by depositing cobalt on alumina from a nitrate solution during the decomposition of urea, $RuNO(NH_3)_2(NO_3)_3$. We establish a relationship between the temperature of cobalt reduction and the amount of applied ruthenium, and describe the properties of the catalyst during FTS.

EXPERIMENTAL

Preparing the Catalyst

Cobalt–alumina catalyst (hereinafter denoted as Co-Al) was prepared by depositing cobalt hydroxy compounds onto alumina during its precipitation from a cobalt nitrate solution under the conditions of urea hydrolysis, a method referred to as deposition precipitation with urea (DPU) [22–24]. Granular cylindrical δ-Al_2O_3 2.5 mm in diameter and 4–5 mm long, obtained by thermally treating pseudoboehmite A64 (OAO AZK & OS, Angarsk) in air at 900°C for 3 h, the

salt $Co(NO_3)_2 \cdot 6H_2O$ (pure grade, GOST (State Standard) 4528-78), and urea (analytical grade, GOST 6691-77) were used in our synthesis. After cobalt deposition, the granules were separated from the suspension, washed thoroughly with distilled water, and dried in air. The chemical and phase composition of the Co-Al catalysts prepared using this approach, and the evolution of their structure during calcination and subsequent reductive activation, were studied in detail in [9, 10]. The prepared $Co/\delta\text{-}Al_2O_3$ catalysts were highly active in FTS.

Ruthenium-promoted catalysts were obtained by impregnating dry Co-Al catalyst granules with $Ru(NO)(NH_3)_2(NO_3)_3$ aqueous solutions [25], followed by drying at 50°C in air for 12 h. The promoted catalysts are referred to below as Co-Ru(0.2)Al, Co-Ru(0.5)Al, and Co-Ru(1.0)Al, where 0.2, 0.5, and 1.0 are the target ruthenium amounts (in wt %) as part of the promoted catalyst.

Thermal Analysis

The thermal curves of the changes in sample weight (TG and DTG) were determined on a Netzsch STA 409 PC from 50 to 900°C in PtIr crucibles; the sample weight was 100 mg. Calcination was performed under argon (40 mL/min) at a heating rate of 2°C/min, while reduction was conducted in a 1 : 1 argon/hydrogen mixture (40 mL/min) at a heating rate of 3°C/min.

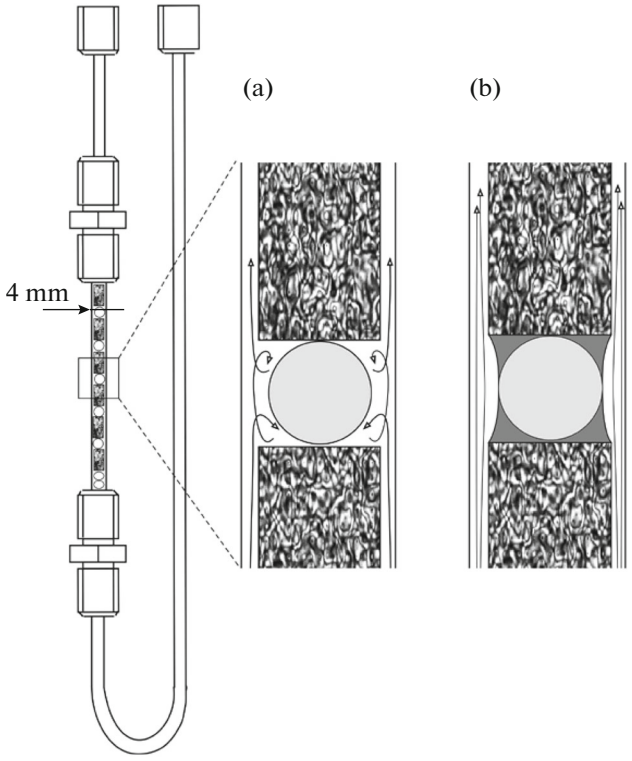

Fig. 1. Scheme of catalyst loading in the Temkin reactor (a) before catalytic tests and (b) after the accumulation of liquids in intergrain area (*see text*). The arrows indicate the direction of the gas flow.

Catalytic Tests

Catalytic tests were performed in a single-row (Temkin) tube fixed-bed reactor 4 mm in diameter (Fig. 1a). Catalyst granules (cylinders 2.5–3 mm in diameter and 5–7 mm long) alternated with alumina balls 2.5–3 mm in diameter to create flow turbulence and avoid possible near-wall effects in the single-row reactor; the overall bed height was about 7 cm. FTS was conducted at 190°C and a pressure of 2.1 MPa. The composition of the initial working mixture (IWM) $H_2 : CO : N_2$ was 6 : 3 : 1, and flow rate of a gas mixture was 3.1 $L_{STP}/(g_{cat}^{-1}\ h)$. The degree of conversion of CO and hydrogen, along with the contents of methane and CO_2 in the gas flow downstream of the reactor were determined by means of chromatography (packed column with activated charcoal, TCD), using nitrogen as an internal standard. The gaseous C_1–C_8 products of synthesis were analyzed via chromatography (FID, capillary column with $\gamma\text{-}Al_2O_3$). The liquid C_{8+} hydrocarbons accumulated during tests in a separator, and the solid products (C_8–C_{40}) accumulated in the reactor volume and extracted with hexane from the catalyst were analyzed on a Tsvet-560 chromatograph equipped with an FID and a capillary column with stationary phase SE-54.

The composition of the gas phase was determined every 40–50 minutes. The total time of the catalytic tests and condensate accumulation with subsequent analysis varied for the different catalysts: Co-Al, Co-Ru(0.2)Al with Co-Ru (0.5)Al, and Co-Ru(1.0)Al required 77, 24, and 43 h, respectively. The composition of the hydrocarbons extracted from the catalyst grains was determined after each experiment. It should also be noted that some products with hydrocarbon chain lengths of 16 to 25 carbon atoms were condensed or adsorbed on the walls of the gas lines connecting the reactor and separator. The scheme of the setup called for heating these lines, but washing the equipment with hexane after tests revealed a considerable amount of products in this range. Their amount was obviously small compared to the products accumulated in the separator and reactor if the test time was long enough. In our case, however, this fraction of products may be significant for the total mass balance during express quality control analysis (nearly 5% of the condensed products found in separator). The products washed out of the reaction system with hexane were therefore analyzed for every catalyst.

Before catalytic tests, the catalysts were activated in a flow reactor under Ar and then in a hydrogen atmosphere at temperatures selected according to the thermal analysis data (TG/DTG) (Table. 1). Calcination and reductive activation were conducted by gradually raising the temperature (2°C/min) up to the selected

Table 1. Experimental data on the amounts of active metal (Co) and promoter (Ru) in dried samples, typical catalyst reduction temperatures according to thermal analysis (T_{start} and T_{max}), and temperatures for their activation in Ar (T_{calc}) and H_2 (T_{red}) before catalytic tests.

Catalyst	Contents in dried sample, wt %		Characteristic reduction temperatures, °C		Catalyst activation temperatures, °C		Weight loss during reduction (TG data), %	
	Co	Ru	T_{start}	T_{max}	T_{calc}	T_{red}	1st stage	2nd stage*
Co-Al	9.53	–	330	550	350	500	2.0	4.5
Co-Ru(0.2)Al	9.20	0.18	228	383	350	350	1.8	4.8
Co-Ru(0.5)Al	9.14	0.45	207	300	330	330	1.7	4.9
Co-Ru(1.0)Al	9.37	0.94	174	267	300	330	1.5	5.4

* Up to 900°C.

value and then maintaining it temperature for 1.5 h during calcination, or for 4 h during reductive activation.

Table 1 summarizes the elemental composition of the catalysts, the characteristic reduction temperatures (DTG data), and the hydrogen activation temperatures prior to catalytic measurements. The characteristic temperature on the thermal curves (T_{max}) is the temperature, at which the maximum rate of change in sample weight was reached during the reduction of the active component at a temperature increase rate of 3°C/min. The temperature can be limited to lower values under the conditions of prolonged activation (4 h) by focusing on the initial temperature of weight loss (T_{start}).

The amount of cobalt in all of the dried Co-Ru(x)Al samples ranged from 9.1 to 9.4 wt %, conforming to the one in the initial catalyst. The content of Ru in the modified samples was 6–10% lower than the theoretical one. The weight loss during calcination in an argon flow with 2°C/min was 14–15% at 300–350°C. The different amounts of Co and Ru, along with the slightly different weight losses, were due to impurity anions and water in the catalysts.

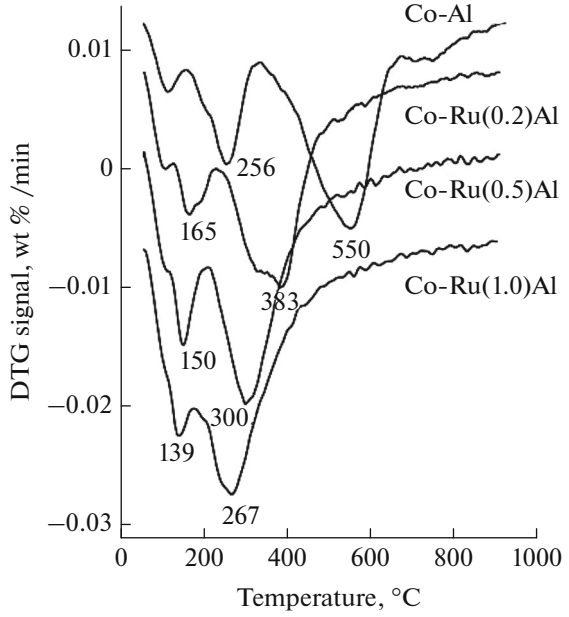

Fig. 2. DTG reduction profiles of Co-Al and Co-Ru(x)Al catalysts in a mixture (50% H_2 and Ar) at a heating rate of 3°C/min. The numbers indicate the temperatures at the maximum rates of conversion (T_{max}).

RESULTS AND DISCUSSION

Figure 2 shows the experimental differential TG (DTG) reduction profiles, depending on temperature. The DTG data indicate that reduction of cobalt from the precursor compounds occured in several stages for all the systems to form Co^0, as is shown in the temperature ranges near the weight loss maxima.

In situ X-ray diffraction data [10] show that the first stage of the reduction of the unpromoted Co-Al catalyst in the temperature range of 200–500°C included the reduction of the spinel-like phase of $Co_3O_4^*$ (cobalt oxide doped with aluminum cations, $Co_{3-x}Al_xO_4$ ($0 < x < 2$)) to form a cobalt oxide (II) phase containing aluminum (III) cations CoO*. The latter then transformed into metal cobalt during second stage at temperatures above 450°C. The maximum rate of metal phase formation was observed at a temperature of 550°C. At a above 700°C, the reduction of Co-Al spinels with high amounts of aluminum occurs, which goes on run up to 1000°C and above. Introducing ruthenium into the cobalt-alumina catalyst shifts the temperature ranges for both stages of reduction, $Co_3O_4^* \rightarrow CoO^* \rightarrow Co$, toward lower temperatures. This effect is more pronounced, if the amount of ruthenium in the catalyst is high. The relationship between the temperature of reduction and the amount of introduced ruthenium is observed to a lesser extent in the first stage of reduction and is more pronounced during the second stage. When we selected our reduction activation temperatures, we were guided by the T_{max} values and roughly the same weight loss values in this area (3.0–3.4%). T_{red} for Co-Ru(0.5)Al and Co-Ru(1.0)Al catalysts were thus

Table 2. Test results for the studied catalysts in the Fischer–Tropsch reaction at 190°C, 2.1 MPa, $H_2 : CO : N_2 = 6 : 3 : 1$, and a feed rate of 3.1 L/(g_{cat} h) within 24 and 43 h after start of tests.

Parameter	Co-Al		Co-Ru(0.2)Al	Co-Ru(0.5)Al	Co-Ru(1.0)Al	
Activation temperature in H_2, °C	500		350	330	330	
Testing time, h	24	43	24	24	24	43
X_{CO}, %	10.5	8.7	8.2	8.3	10.4	6.6
W_{CO}, mmol/(g_{cat} h)	4.3	3.5	3.5	3.4	4.3	2.7
$S(CH_4)$, %	10.0	17.5	9.5	9.3	9.9	19.5
$S(C_{5+})$, %	78	74	77	79	79	68
Propene/propane yield ratio	1.5	0.75	3.0	2.6	2.5	0.5
Decene/decane yield ratio	0.22		0.18	0.15	0.17	
α_{ASF} Parameter for C_{28}–C_{39} paraffin fraction	0.89		0.93	0.93	0.94	

selected to be higher than T_{max}, while the opposite was true for Co-Al and Co-Ru (0.2)Al.

Table 2 and Figs. 3–7 show the results from catalytic tests for the catalysts reduced at 330–500°C.

Figure 3 shows the relationship between the degree of CO conversion and selectivity toward methane and the duration of an experiment. A periodic decrease in activity and an increase in selectivity toward methane observed especially in Fig. 3a was due to stopping the test for the night to cool the reactor and continuing the tests after heating it again in the morning. The conversion over Co-Al catalyst remained within ±1–2% over 27 h and 32 h for the Co-Ru(1.0)Al sample. The observed activity of the catalyst then fell by 20–35%, and the selectivity toward methane was doubled. We assume that a decrease in the activity of the catalysts and the change in the process's selectivity were not due to the deactivation of the catalyst, but to the diffusion limitations of the reactants through the high molecular hydrocarbon phase accumulated in the reactor, not only in the catalyst pores but in the intergranular space of the reactor as well. We estimate that the volume of the liquid product accumulated in the reaction volume (see. Fig. 3) was considerably greater than free volume of the catalyst pores at the time when the activity fell. As a result, by that time there was a liquid phase of the products between the catalyst grains. Distribution of this phase in the reaction volume (Fig. 1b) was initially limited by the menisci between the catalyst cylinders and the aluminum oxide balls. Such a structure of the catalyst bed in a single-row reactor can no longer ensure reliable determination of the activity and selectivity of catalysts, since the gas flow becomes laminar and the wall effect is very significant.

Diffusion limitations affects not only the reaction rate but the process selectivity as well [26, 27]. When diffusion limitations becomes strong, the ratio of H_2 : CO concentration rises within the pores of the catalyst grain, leading to greater selectivity toward methane. Diffusion limitations becomes also stronger for the process of removing of α-olefins from the pores of the catalyst grains, which can result in their readsorption and subsequent hydrogenation to form alkanes. This

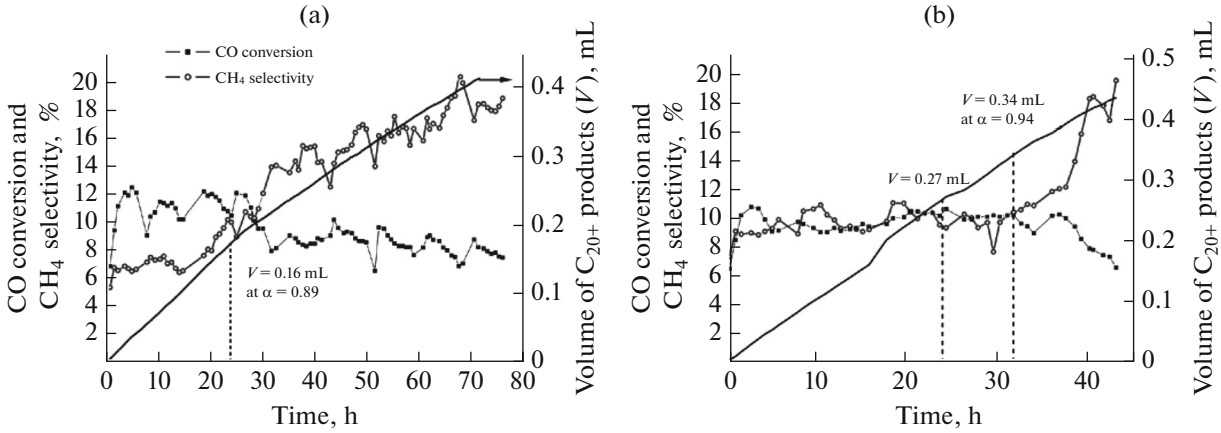

Fig. 3. CO conversion and CH_4 selectivity time of an experiment, compared to the amount of liquid hydrocarbons in the volume of the reactor over (a) Co-Al and (b) Co-Ru(1.0)Al.

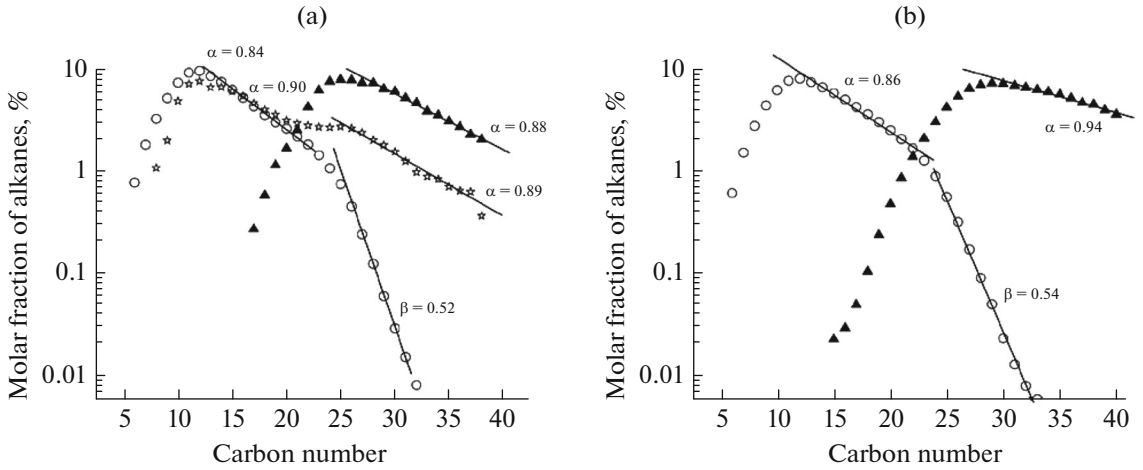

Fig. 4. Experimental data on the composition of products in the condensed phase: (○) from the separator, (▲) extracted from catalyst after the end of tests, and (*) in the hexane used to wash the system after tests; (a) Co-Al, (b) Co-Ru(1.0)Al.

was confirmed by a drop in the yield of olefins in the gas phase after 43 h of catalyst action (Table 2).

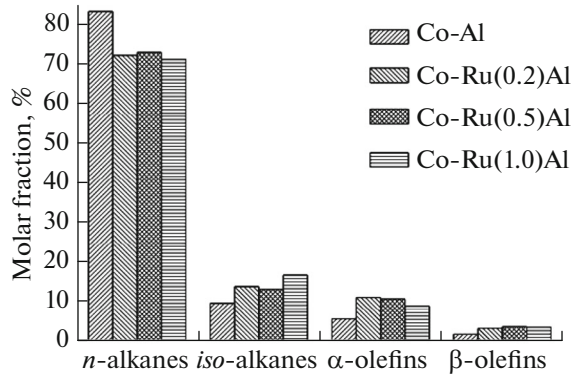

Fig. 5. Distribution of the C_{10}–C_{14} fraction of FTS products by their chemical nature.

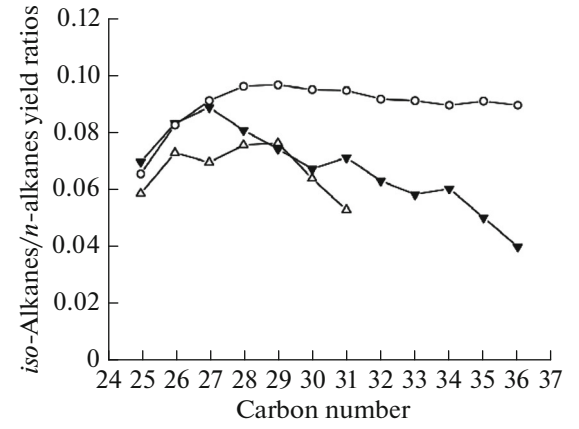

Fig. 6. *iso*-Alkanes/*n*-alkanes ratio in the C_{25+} fraction of FTS products versus hydrocarbon chain length: (○) Co-Al, (△) Co-Ru(0.2)Al, (▲) Co-Ru(1.0)Al.

In light of the above, we shall rely on the results from the catalytic tests performed over the first 24 h when considering the role of ruthenium promotion. When the conversion of CO on the Co-Al catalyst was 10.5%, the rate of CO conversion (W_{CO}) was 4.3 mmol CO/(g_{cat} h). For the catalysts modified by 0.2 and 0.5 wt % of Ru, the conversion was less by 20% (8.2–8.3%) and W_{CO} was 3.4–3.5 mmol CO/(g_{cat} h). The activity of the Co-Al catalyst promoted with 1.0 wt % of Ru was, however, higher than those with 0.2–0.5% ruthenium and was close to the activity of the unpromoted Co-Al catalyst. The promotion of catalysts with ruthenium from ammine(nitrato)nitrosoruthenium complexes thus allows us to lower the temperature of reductive activation from 500 to 330–350°C with or without a slight drop in the specific activity of the catalyst. The activation temperatures selected for the Co-Ru(0.2)Al and Co-Ru(0.5)Al catalysts could be less than optimal, and raising some of them would have a positive impact on the activities of these catalysts.

The impact of uthenium on the selectivity of catalysts deserves our attention. Selectivity toward the C_{5+} fraction was 77–79% for all the samples and was 9.3–10% toward methane. The selectivity of the ruthenium-promoted catalysts toward high molecular hydrocarbons was, however, considerably higher. Figure 4 shows the relationship between the relative amounts of C_{5+} alkanes in a condensate and in an extract obtained from catalyst granules after a reaction and the hydrocarbon chain length. The α_{ASF} values of the ruthenium-promoted samples (0.93–0.94) are appreciably higher than that of the Co-Al catalyst (0.88).

The α_{ASF} values for the C_{12}–C_{22} fractions, determined from the composition of condensate, were slightly lower than those of C_{28}–C_{39} fractions, determined from the composition of an extract of catalyst granules. Sometimes this deviation, described as a flat or double Flory, is due to differences in selectivity

between active sites (e.g., a bimodal distribution of active ingredient particles according to size) or stronger diffusion limitations of high molecular olefins, resulting in their readsorption, hydrogenation, and a rise in the α_{ASF} value. In our case, however, we believe that the liquid hydrocarbon/gas–vapor phase equilibrium in the reaction volume at 190°C affected the observed α_{ASF} value for C_{12}–C_{22} from condensate [28]. The longer the carbon chains, the greater the proportion of hydrocarbons that remains in the liquid phase. Strictly speaking, phase equilibrium in a hydrocarbon mixture does not conform to the laws of ideal mixtures, and the dependence of the pressure of saturated vapor over a liquid phase on its composition is complicated [29]. The relationship between saturated vapor pressure over pure hydrocarbon and the length of hydrocarbon chains is also complex, but we may assume with a reasonable degree of certainty that it reduces exponentially:

$$\ln P_n^0 = a - bn, \quad (3)$$

$$P_n^0 = A\beta^n. \quad (3a)$$

If the reactor temperature is 190°C, exponent b of this relationship can be estimated for C_{21}–C_{30} hydrocarbons as −0.455, while the parameter $\beta_{190\,C} \approx 0.63$ [30]. The effect of the hydrocarbon chain length on the pressure of saturated vapor in contact with a liquid phase is clearly seen on the condensate composition curves of C_{25+}. In this range, the base value of exponential function β_{obs} is $\approx\beta_{190\,C} \cdot \alpha_{ASF}$, and is therefore less than 0.63. In the C_{12}–C_{22} range, the fraction of hydrocarbons accumulated with a liquid phase in equilibrium with a vapor–gas phase at a reactor temperature of 190°C rising along with the hydrocarbon chain length, becomes significant at C_{17+} and thus lowers the α_{ASF} distribution parameter determined from an analysis of the condensate.

The composition of the FTS reaction products can be estimated by summing the hydrocarbons found in the condensed phases. The accuracy of determining the total amount of condensate and extracted substances in our experiments is, however, insufficient for evaluation. For illustrative purposes, we have experimental data on the content of hydrocarbons in the hexane (Fig. 3) used to wash the reaction system after tests. This solution contained C_{10}–C_{36} hydrocarbons. It is noteworthy that the α_{ASF} value for the C_{15}–C_{22} hydrocarbon fraction in this sample was 0.90, slightly higher than the one for C_{28+}. This indicates the α_{ASF} values obtained via condensate analysis were underestimated, and the actual α_{ASF} value probably differed less for the C_{15}–C_{22} and C_{28+} hydrocarbons. It should be noted that the considerable impact of phase equilibrium on the α_{ASF} value determined from composition of the condensate was due to the difference between the reaction temperature (190°C) and the temperature of the condensation products (60°C). If the reaction proceeds at 210°C, the molecular-weight distribution of hydrocarbons in the condensate at 60°C allows us to select the area in which the observed α_{ASF} value describes the actual selectivity of the process.

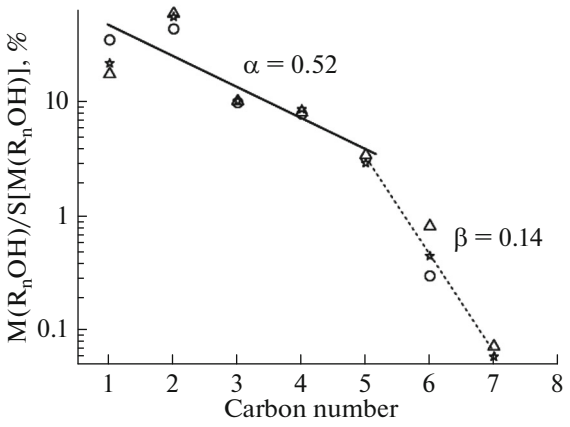

Fig. 7. Distribution of alcohols in the aqueous fraction of Fischer–Tropsch products, according to the number of carbon atoms: (○) Co-Al, (△) Co-Ru(0.2)Al, and (*) Co-Ru(0.5)Al.

Ruthenium-promoted catalysts yield high amounts of olefins in the products of a reaction: the promoted samples had almost twice the α-olefin/corresponding alkane ratio (the C_3 and C_{10} data in Table 2). Figure 5 shows the ratio of the amounts of linear alkanes, branched alkanes, α-olefins, and β-olefins in the C_{10}–C_{14} hydrocarbons according to our analysis of the condensate for the promoted and unpromoted catalysts, presented as histograms.

Ruthenium promotion raised the selectivity of the catalysts relative to branched hydrocarbons and olefins. The drop in catalyst activity during ruthenium promotion correlates with the increase in selectivity toward olefins and testifies to the lower hydrogenation ability of an active component. It is worth noting that the C_{25+} high molecular hydrocarbon fraction has no olefins. Figure 6 shows the ratio of linear alkanes to branched alkanes. The amount of the branched alkanes in C_{25+} hydrocarbons obtained on ruthenium catalysts is no more than 9%, and ruthenium reduces the proportion of branched alkanes in this fraction. We are currently unable to explain the effect of ruthenium on the composition of high molecular waxes.

Alcohols formed along with hydrocarbons during the Fischer–Tropsch reaction. Chromatographic analysis of the aqueous fraction of the products revealed C_1–C_7 alcohols (Fig. 7). The distribution of alcohols according to the number of carbon atoms can be described with ASF distribution parameter α_{alc} as ±0.52. The solubility of alcohols in water is reduced rapidly as the number of carbon atoms in them rises,

so the amount of C_{6+} alcohols is negligible in the aqueous fraction. Figure 7 indicates that ruthenium promotion has no noticable effect on selectivity with respect to the formation of alcohols. According to our estimates, the overall yield of alcohols was around 3% for all of the catalysts, whether they were ruthenium-promoted or not.

CONCLUSIONS

Introducing ruthenium (up to 1 wt %) into Co-Al catalyst by impregnating with ammine(nitrato)nitrosoruthenium complexes substantially lowers the required temperature of reduction activation from 500 to 330°C while preserving high catalytic activity and selectivity toward C_{5+} products during the reaction of Fischer–Tropsch synthesis. The catalytic activity is 3.5–4.3 mmol CO/(g_{cat} h) at 190°C, 2.0 MPa, and 10.8% conversion of CO, while the selectivity to C_{5+} products is 77–79%.

Ruthenium-promoted Fischer–Tropsch Co-Al catalysts were more selective toward higher hydrocarbons: experimental parameter α_{ASF} for the distribution of paraffinic products was 0.93–0.94. This allows us to estimate the selectivity toward C_{20+} synthetic waxes to be 48 wt %, and the selectivity toward C_{35+} waxes to be 23 wt %. Ruthenium-promoted catalysts also exhibited high selectivity toward olefins.

ACKNOWLEDGMENTS

The authors are grateful to Prof. V.A. Emelyanov (Novosibirsk State University), who afforded $Ru(NO)(NH_3)_2(NO_3)_3$ complex for the study.

This work was supported by the Joint Research and Educational Center for Energy Efficient Catalysis (Novosibirsk State University and Boreskov Institute of Catalysis, SB RAS), and russian government decree no. V.45.3.6.

REFERENCES

1. Lisitsyn, A.S., Golovin, A.V., Kuznetsov, V.L., and Yermakov, Yu.I., *C_1 Mol. Chem.,* 1984, no. 1, pp. 115–135.
2. Khassin, A.A., Yur'eva, T.M., and Parmon, V.N., *Dokl. Phys. Chem.,* 1999, vol. 367, nos. 1–3, pp. 213–216.
3. Satterfield, C.N., Huff, G.A., Stenger, H.G., Carter, J.L., and Madon, R.J., *Ind. Eng. Chem. Fundam.,* 1985, vol. 24, no. 3, pp. 450–454.
4. Tavasoli, A., Pour, A.N., and Ahangari, M.G., *J. Nat. Gas Chem.,* 2010, vol. 19, no. 6, pp. 653–659.
5. Savost'yanov, A.P., Narochnyi, G.B., Yakovenko, R.E., Bakun, V.G., and Zemlyakov, N.D., *Catal. Ind.,* 2014, vol. 6, no. 4, pp. 292–297.
6. Ermolaev, I.S., Ermolaev, V.S., and Mordkovich, V.Z., *Theor. Found. Chem. Eng.,* 2013, vol. 47, no. 2, pp. 153–158.
7. Sineva, L.V., Mordkovich, V.Z., Ermolaev, V.S., Ermolaev, I.S., Mitberg, E.B., and Solomonik, I.G., *Katal. Prom-sti,* 2012, no. 6, pp. 13–22.
8. Lamprecht, D., Nel, R., and Leckel, D., *Energy Fuels,* 2010, vol. 24, no. 3, pp. 1479–1486.
9. Simentsova, I.I., Khassin, A.A., Minyukova, T.P., Davydova, L.P., Shmakov, A.N., Bulavchenko, O.A., Cherepanova, S.V., Kustova, G.N., and Yurieva, T.M. *Kinet. Catal.,* 2012, vol. 53, no. 4, pp. 497–503.
10. Khassin, A.A., Simentsova, I.I., Shmakov, A.N., Shtertser, N.V., Bulavchenko, O.A., and Cherepanova, S.V., *Appl. Catal., A,* 2016, vol. 514, pp. 114–125.
11. RF Patent 2538088, *Byull. Izobret.,* 2015, no. 1.
12. Simentsova, I.I., Khasin, A.A., Shtertser, N.V., Davydova, L.P., Minyukova, T.P., and Yur'eva, T.M., *Katal. Prom-sti,* 2016, no. 2, pp. 17–22.
13. Khassin, A.A., Anufrienko, V.F., Ikorskii, V.N., Plyasova, L.M., Kustova, G.N., Larina, T.V., Molina, I.Yu., and Parmon, V.N., *Phys. Chem. Chem. Phys.,* 2002, vol. 4, no. 17, pp. 4236–4243.
14. Tsubaki, N., Sun, S., and Fujimoto, K., *J. Catal.,* 2001, vol. 199, no. 2, pp. 236–246.
15. Ma, W., Jacobs, G., Keogh, R.A., Bukur, D.B., and Davis, B.H., *Appl. Catal., A,* 2012, vols. 437–438, pp. 1–9.
16. Jacobs, G., Das, T.K., Zhang, Y., Li, J., Racoillet, G., and Davis, B.H., *Appl. Catal., A,* 2002, vol. 233, nos. 1–2, pp. 263–281.
17. Song, S.-H., Lee, S.-B., Bae, J.W., Sai Prasad, P.S., and Jun, K.-W., *Catal. Commun.,* 2008, vol. 9, no. 13, pp. 2282–2286.
18. Kogelbauer, A., Goodwin, J.G., and Oukaci, R., *J. Catal.,* 1996, vol. 160, no. 1, pp. 125–133.
19. Park, J.-Y., Lee, Y.-J., Karandikar, P.R., Jun, K.-W., Bae, J.W., and Ha, K.-S., *J. Mol. Catal. A: Chem.,* 2011, vol. 344, nos. 1–2, pp. 153–160.
20. Parnian, M.J., Najafabadi, A.T., Mortazavi, Y., Khodadadi, A.A., and Nazzari, I., *Appl. Surf. Sci.,* 2014, vol. 313, pp. 183–195.
21. Cook, K.M., Poudyal, S., Miller, J., Bartholomew, C.H., and Hecker, W.C., *Appl. Catal., A,* 2012, vol. 449, pp. 69–80.
22. Hermans, L.A.M. and Geus, J.W., *Stud. Surf. Sci. Catal.,* 1979, vol. 3, pp. 113–130.
23. Bezemer, G.L., Radstake, P.B., Koot, V., van Dillen, A.J., Geus, J.W., and de Jong, K.P., *J. Catal.,* 2006, vol. 237, no. 2, pp. 291–302.
24. Eschemann, T.O., Bitter, J.H., and de Jong, K.P., *Catal. Today,* 2014, vol. 228, pp. 89–95.
25. Emel'yanov, V.A., Formation and conversion of ruthenium nitrozo complexes in chloride, nitrite, nitrate, and ammonia solutions, *Doctoral (Chem.) Dissertation,* Novosibirsk: Nikolaev Inst. Inorg. Chem., 2013.
26. Iglesia, E., Reyes, S.C., and Madon, R.J., *J. Catal.,* 1991, vol. 129, no. 1, pp. 238–256.
27. Iglesia, E., *Appl. Catal., A,* 1997, vol. 161, nos. 1–2, pp. 59–78.
28. Zhan, X.D. and Davis, B.H., *Pet. Sci. Technol.,* 2000, vol. 18, nos. 9–10, pp. 1037–1053.
29. Derevich, I.V., Ermolaev, V.S., Zol'nikova, N.V., and Mordkovich, V.Z., *Theor. Found. Chem. Eng.,* 2013, vol. 47, no. 3, pp. 191–200.
30. Chickos, J.S. and Hanshaw, W., *J. Chem. Eng. Data,* 2004, vol. 49, no. 1, pp. 77–85.

Translated by A. Tulyabaev